ENERGY QUIPSYS

Energy Equipment and Systems

ENERGY QUIPSYS

ENERGY EQUIPMENT AND SYSTEMS

Electromagnetic field analysis of novel low cogging force, linear switched reluctance motor, based on 2-D finite element method

Authors

Hassan Moradi CheshmehBeigi [a]

[a] Electrical Engineering Department, Faculty of Engineering, Razi University, Kermanshah 67149, Iran

ABSTRACT

This paper deals with electromagnetic design and 2-D (two-dimensional) magnetic field analysis of novel low force ripple linear switched reluctance (LSR) motor. The configuration that has been presented here has a higher number of rotor poles than stator poles, and the purpose of this configuration is to improve the force ripple, which is the weak point of LSRMs. In order to illustrate the conformity of the design parameter's stage in this study, the calculated values of the magnetic field and cogging force characteristics are compared with that of their desired values. Also, the proposed configuration is compared to a 6-4 and 3-phase conventional LSRM with similar number of stator teethes, number of phases, and constraints in volume. From the numerical analysis of a proposed novel configuration, it has been observed that this machine produces higher force per unit volume and almost similar cogging force when compared to a conventional LSRM with identical number of stator teethes, number of phases, and constraints in volume. The obtained primary electric and magnetic characteristics for the proposed configuration are verified with the help of 2-D FE computations.

1. Introduction

Linear Switched reluctance motors (LSRMs) are attractive due to their simple structure, low cost in mass production, high performance and efficiency, lesser maintenance requirement, fault tolerance, rugged motor construction, high force over a wide speed range, and easy speed control [1–4]. Hence, due to these advantages, during the past few decades LSRM has been the focus of intensive research efforts for variable speed application in industries [5, 6]. However, it has an inherent high cogging force due to its salient structure, which results in an undesirable acoustic noise and mechanical vibration. In order to apply LSRM and SRM to the industrial field, the force ripple has to be reduced [7, 8]. Rotary SRM torque ripple reductions have been investigated in many studies using two main approaches, the geometric design parameter change and electronic control strategies. The geometric design approach is based on optimizing the salient pole shapes, especially salient pole arc, such as stator pole arc (β_s) and rotor pole arc (β_r) [9–11]. The electronic control strategy is based on the selection of an

*Corresponding author: Hassan Moradi CheshmehBeigi
Address: Electrical Engineering Department, Faculty of Engineering, Razi University, Kermanshah 67149, Iran
E-mail address: ha.moradi@razi.ac.ir

optimum combination of electric design parameters, such as turn on and turn off angles (θ_{on} and θ_{off}), level of current, and supply voltage [12–15]. A novel stator pole shape with non-uniform air-gap and a pole shoe on rotor pole to reduce the torque ripple was investigated in [16, 17]. A new hybrid stator-pole that improves the radial force is described in [18]. This paper presents electromagnetic design and magnetic field analysis, and predicts the electromagnetic behavior of a novel configuration linear switched reluctance motor, which has a higher number of rotor poles than stator poles. The purpose of this configuration is to improve cogging force. To predict the electromagnetic behavior and estimate the overall performance of the proposed novel configuration, 2-D finite element method has been utilized.

Numerical techniques, such as FE computation, can be utilized for modeling and predicting the electromagnetic behavior, especially in novel configurations studies for different operation modes. The electromagnetic characteristics, such as inductance, terminal induced Back-EMF, precise flux linkage, and mutual inductance, can be obtained by magnetic field computation inside the machine. FE method utilizes materials property, machine geometry, and all the boundary conditions for magnetic field computation.

Numerical techniques, such as Finite Element Method (FEM), is suggested by different researchers for modeling and parameter identification of electrical machines [19–25]. In a reference [26], a novel topology of tubular motor with a modular construction and high specific thrust that can be used for various applications has been presented. Again, in another reference [27], an electromagnetic design and 3-D magnetic field analysis of a novel configuration machine based on a hybrid analytical, assisted by BLDC field and 3-D FEM analysis has been presented. In this paper, the design methodology obtained primary magnetic and electric characteristics for the configuration under study and is verified by 3-D FE computation. The design and analysis of a two double-rotor flux-modulated permanent-magnet machine for direct-drive applications by using the time-stepping finite element method has been presented in a reference [28]. A reference [29] showed the development of MGs. Hence, in this study, the MGPM machines have been presented and discussed, with emphasis on providing

performance analysis and a quantitative comparison of three viable MGPM machines. A novel double-winding flux-modulated permanent magnet machine (FMPM) for stand-alone wind power generation is presented in reference 30. The results showed that the proposed FMPM has a higher torque capability and stronger flux adjustability than the existing single-winding FMPMs. In reference 31, a novel dual Halbach array has been proposed to enhance flux density in the air gap, thus improving the output performance of linear machines. In this paper, the numerical results from finite element method are employed to simulate and observe the flux distribution in the machine. In a reference [32], the design and analysis of an inside-out axial-flux permanent magnet (AFPM) synchronous machine optimized by genetic algorithm (GA) based sizing equation, finite element analysis (FEA), and finite volume analysis (FVA) has been demonstrated. The modeling of the brushed DC motor used as a reinforced starter for a micro-hybrid automotive application has been presented in reference 33. The design criteria for a tubular linear induction motor (TLIM) as fast actuators has been shown in reference 34. The influence of geometrical and physical parameters on the operating conditions of a TLIM are investigated by the means of a quasi-analytic model.

This paper is organized as follows: The introduction is presented in Section I. Section II of the paper focuses on the principle operation of the proposed novel structure. Dynamic mathematical model is presented in section III. The sections thereafter describe different ways of obtaining the flux-linkage characteristics for SRM and LSRM. Section V describes design calculations of the proposed 6/10 three-phase LSRM. The subsequent sections describe numerical analysis and discussion on magnetic field for the proposed SR machine. The detailed simulation and magnetic optimization are presented in section VII. The conclusion is presented at the end.

2. Principle operation of proposed novel structure

The principle operation of LSRM is similar to the rotary switched reluctance motor (RSRM). It should be noted that the LSRM produces linear force and RSRM produces rotational torque. It can be assumed that LSRM is merely a 'rolled out' version of a RSRM. In LSRM, the translator (or rotor) is the moving

part and the stator is the stationary part in which linear force production occurs due to the tendency of the translator to move towards a separate stationary point where the inductance of the excited winding is maximum. During the past few decades, several configurations for the LSRM, including various combinations of rotor and stator poles, have been studied [1]. Some well-known configurations of regular stator and rotor poles are given as Table 1.

The proposed configuration in this paper is an LSRM with more rotor poles than stator poles.

This LSRM consist of salient pole in both of stator, with six salient poles (N_s) and translator, with ten salient poles (N_r). In the proposed configuration, the number of turns in each phase has been increased because of the availability of more slot area. Hence, it was possible to increase the overall force per unit volume. In this configuration, bth the stator and translator consist of stacked laminations. The stator consists of stacked laminations with concentrated winding wrapped around the salient poles. Figure 1 shows the complete assembly of the proposed 6-10 machine with phase winding. Figure 2 shows the complete assembly of the conventional 6-4 machine with phase winding.

Understudy conventional LSRM is a 3-Phases and 6-4 configuration, consist of salient pole in both of stator, with six salient poles (N_s) and translator, with four salient poles (N_r).

Table 1. Several LSRM configurations with regular stator and rotor poles.

	Phase Number	N_s/N_r						
1	Three-Phase	6/2	6/4	6/8	6/14	12/8	18/12	24/16
2	Four-Phase	8/6	8/10	16/12	24/18	32/24		
3	Five-Phase	10/4	10/6	10/8	10/12			
4	Six-Phase	12/10	12/14	24/20				
5	Seven-Phase	14/10	14/12	14/16				
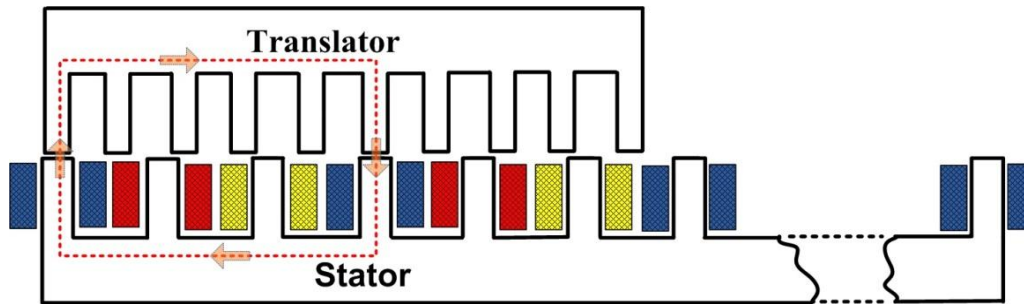
**Fig. 1.** Complete assembly of proposed 6-10 LSRM with phase winding
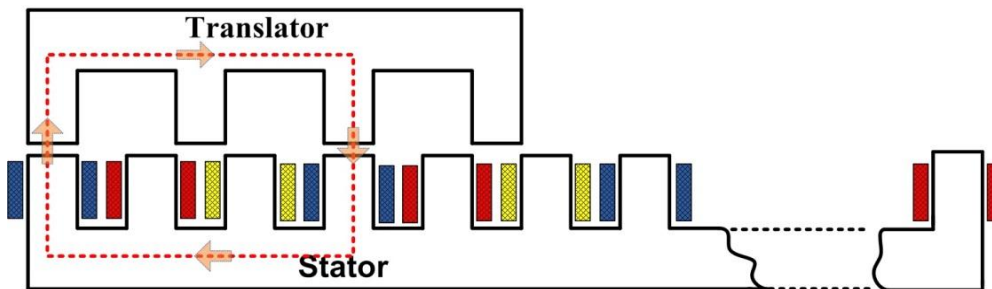
Fig. 2. Complete assembly of proposed 6-4 LSRM with phase winding

3. Dynamic mathematical model

Mathematical equations of the electric circuit for each phase, and mechanical part of the LSRM are the basis of the dynamic model [35, 36]. Flux-linkage characteristics and its derivatives are required for simulation of the LSRM, based on the dynamic mathematical model. Special attention should be paid to its determination to ensure reliability of the obtained model. The mathematical equations and dynamic model of SRM and LSRM per phase are given as Table 2.

Table 2. The mathematical equations and Dynamic Model of SRM and LSRM Per Phase

The Mathematical Equations Of The Electric Circuit
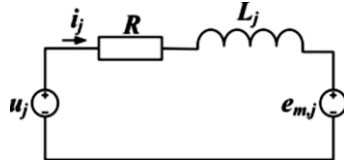
Electrical Equivalent Circuit Per Phase of an LSRM

The Voltage Phase Equation:	$u_j = \dfrac{\partial \psi_j(x, i_j)}{\partial t} + R i_j$ $= \underbrace{\dfrac{\partial \psi_j(x, i_j)}{\partial i}}_{L_j} \dfrac{di_j}{dt} + R i_j$ $+ \underbrace{\dfrac{\partial \psi_j(x, i_j)}{\partial x}}_{e_{m,j}} v$ $u_j = L_j \dfrac{di_j}{dt} + e_{m,j} + R i_j$	R: Phase resistance L_j: Inductance ψ_j: Flux linkage u_j: Applied voltage F_e: Electromechanical force produced F_l: Mechanical load F_r: Friction M: Translator mass v: Velocity x: Position
Instantaneous Electromagnetic Force (F_e) Per Phase	$F_e = \sum_{j=1}^{m} \left(\dfrac{\partial}{\partial x} \left(\int_0^I \psi_j(x, i_j)\, di_j \right)_{I=ctn} \right)$ $F_e = M \dfrac{dv}{dt} + F_r + F_L$ $v = \dfrac{1}{M} \int (F_e - F_r - F_L) . dt$	
Dynamic Model of LSRM Per Phase	$\dfrac{di_j}{dt} = \left(\dfrac{\partial \psi_j(x, i_j)}{\partial i_j} \right)^{-1} \left(u_j - R i_j - \dfrac{\partial \psi_j(x, i_j)}{\partial x} v \right)$ $\dfrac{dv}{dt} = \dfrac{1}{M} (F_e - F_r - F_L)$ $i_j = \int \left(\dfrac{\partial \psi_j(x, i_j)}{\partial i_j} \right)^{-1} . \left(u_j - R i_j - \dfrac{\partial \psi_j(x, i_j)}{\partial x} v \right) dt$	
Dynamic Model of Rotary SRM Per Phase	$\dfrac{di_j}{dt} = \dfrac{1}{\dfrac{d^2 W_{co}(i_j, \alpha)}{di^2}} \left(u_j - R i_j \right.$ $\left. - \dfrac{d^2 W_{co}(i_j, \alpha)}{di_j\, d\alpha} \omega \right)$ $T_e(i, \alpha) = \dfrac{dW_{co}(i_j, \alpha)}{d\alpha} = J \dfrac{d^2 \alpha}{dt^2} + B \dfrac{d\alpha}{dt} + T_l$ $W_{co}(i_j, \alpha) = \int_0^i \lambda(i_j, \alpha)\, di$	α: The rotor position. ω: The angular velocity. W_{co}: The co − energy. T_e: The instantaneous electromagnetic T_l: The load torque. J: The moment of inertia. B: The coefficient of friction

4. The different was of obtaining flux-linkage characteristics for SRM and LSR

Table 3 presents the three different ways of obtaining flux-linkage characteristics or magnetization curves, two of them are based on FEA and the last one on experimental measurements, which validate previous finite element (FE) methodologies.

5. Design calculation of proposed 6/10 three-phase LSRM

The proposed design procedure utilizes the rotating switched reluctance machine design by converting the specifications of the linear machine into those of an equivalent rotating machine. The machine design is carried out in the rotary section, which is then transformed back into the linear section. The proposed configuration is designed with the following specifications (Table 4).

The acceleration (maximum acceleration if $t_a = t_d$) is:

$$a_a = \frac{v_m}{t_a} \tag{1}$$

The force for initial acceleration is calculated as:

$$a_g = 9.8 \, ^m/_{s^2} \tag{2}$$

$$F_a = M_t.\left(a_a + a_g\right) \tag{3}$$

if deceleration $a_d = -0.6 \, ^m/_{s^2}$.
Instantaneous deceleration force is given as:

$$F_a = M_t.\left(a_a + a_g\right) \tag{4}$$

Maximum power capacity of the LSRM (if $f_f = 0$) as:

$$\begin{cases} P = F_a.v_m \\ P = k_e k_d k_1 k_2 B_g A_{sp} D^2 L N_r \\ L = KD \\ P = k_e k_d k_1 k_2 B_g A_{sp} D^2 v_m \dfrac{60}{\pi} \end{cases} \tag{5}$$

Table 3. Three different ways of obtaining flux-linkage characteristics

Different Ways of Obtaining Flux-Linkage Characteristics

2D FE Model	$$\psi_{2D} = N_{PP} N \oint_C \bar{A}d\bar{l}$$ $$\begin{cases} Range\ of\ position \quad x \quad \overset{\Delta s}{\Rightarrow} \begin{cases} x = 0 & (Fully\ unaligned) \\ x = s & (Full\ aligned) \end{cases} \\ Density\ Current \quad J \quad \overset{\Delta j}{\Rightarrow} \ 0\ to\ 15\ A/mm^2 \end{cases}$$ $$\begin{cases} Range\ of\ position \quad x \quad \Rightarrow \begin{cases} x = 0 & (Fully\ unaligned) \\ x = s & (Full\ aligned) \end{cases} \\ Density\ Current \quad J \quad \overset{\Delta j}{\Rightarrow} \ 0\ to\ 20\ A/mm^2 \end{cases}$$
3D FE Model	$$\psi_{3D}(x,i) = \frac{N_{PP} N}{i} \iiint \bar{A}\bar{J}dV$$ N_{PP} Pole-Coil, N Turn per coil , The current is obtained by: $$i = \iint_S \bar{J}.d\bar{s}$$
Experimental measurements	Experimental measurements validate previous finite element (FE) methodologies.

Table 4. Specifications of Proposed LSRM

L_t	Stator Length of LSRM	1 m
V_m	Maximum Linear Velocity	0.9 m/sec
t_a	Acceleration Time	1.5 sec
M_t	Maximum Mass of Translator Assembly	35 kg
t_d	Deceleration	- 0.6 m/sec^2

The bore diameter is obtained from the power output equation:

$$D = \sqrt{\frac{P\pi}{60 k_e k_d k_1 k_2 B_g A_{sp} v_m}} \tag{6}$$

$$C_{sy} = \frac{D\beta_s}{2} \tag{7}$$

$$h_s = \frac{D_0}{2} - \frac{D}{2} - C_{sy} \tag{8}$$

$$C_{ry} = \frac{D\beta_r}{2} \tag{9}$$

$$h_r = \frac{D}{2} - g - C_{ry} \tag{10}$$

$$\phi = B_g A_g \tag{11}$$

$$A_g = \left(\frac{D}{2} - g\right)\left(\frac{\beta_r + \beta_s}{2}\right) L \tag{12}$$

$$H_g = \frac{B_g}{\mu_0} \tag{13}$$

Ampere-turns required producing the air gap magnetic field intensity

$$\begin{cases} T_{ph} I_P = H_g . 2g \\ T_{ph} = \dfrac{H_g . 2g}{I_P} \\ a_c = \dfrac{I_P}{J\sqrt{m}} \end{cases} \tag{14}$$

$$W_{sp} = C_{ry} \tag{15}$$

$$W_{tp} = C_{sy} \tag{16}$$

where A_g: cross-section area of the air gap, W_{sp}: stator pole width, W_{ss}: stator slot width, W_{tp}: translator pole width, W_{ts}: translator slot width, C_{sy}: stator yoke thickness, h_s; height of the stator pole, C_{ry}: translator yoke thickness, H_g: magnetic field intensity, J: current density, T_{Ph}: number of winding turns per phase, I_P: phase current, a_c: conductor area, m: phase number, ϕ: motor flux linkage, β_s: stator pole angle, β_r: translator pole angle, k_e: efficiency, k_d: duty cycle, $k_1 = \frac{\pi^2}{120}$, k_2: a variable dependent on aligned saturated inductance and unaligned inductance, B_g: air gap flux density, A_{sp}: specific electric loading, D: bore diameter, L: stack length, and N_r: rotor speed. The dimensions of the designed three phases LSRM is shown in Fig.3.
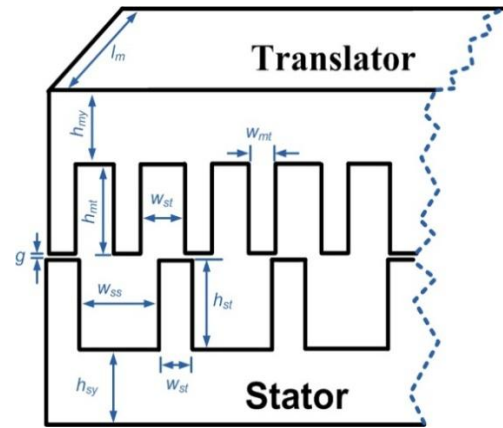

Fig. 3. Dimensions of the designed three-phase LSRM

The calculated design parameters of the proposed 6-10 and conventional 6-4 LSRM are summarized as follow (Table 5).

Table 5. Design specifications of both the motors

Items	6-10 LSRM	6-4 LSRM
Translator width, l_m(mm)	60	60
Translator tooth width, w_{mt} (mm)	19	30
Translator slot width, w_{st} (mm)	21	54
Translator tooth high, h_{mt}(mm)	25	25
Translator yoke high, h_{my}(mm)	20	20
Stator tooth width, w_{st} (mm)	20	28
Stator slot width, w_{ss} (mm)	55	28
Stator tooth high, h_{st}(mm)	30	30
Stator yoke high, h_{sy}(mm)	23	23
Air gap length, g (mm)	0.8	0.8
Number of turns per coil, N_{coil}	220	198
Rate current, I_{RMS} (A)	11	14

6. Numerical analysis of magnetic field for the proposed SR machine

For an accurate calculation of the magnetic field distribution, prediction of the characteristics of machine magnetization and design validation of the proposed machine with the help of complex geometry and nonlinear properties, and numerical technique must be carried out. As mentioned in section IV, FEM is one of the most popular numerical calculation techniques for electromagnetic fields, which have been widely developed for magnetic analysis of electrical machines. In this paper, 2-D FEM is utilized for the calculation and analysis of electromagnetic fields, in and around the proposed configuration. Precise information and electromagnetic characteristics obtained from FE computation is utilized to confirm and describe the principle operation and magnetic behavior of the proposed novel configuration. In this study, $T - \Omega$ formulation, which is a common method for solving magnetic field problems, has been utilized for electromagnetic field solution. In $T - \Omega$ formulation, T defined as [37, 38]:

$$j = \nabla \times T \tag{17}$$

From Maxwell's equation we have:

$$j = \nabla \times T = \nabla \times H \tag{18}$$

Then:

$$\nabla \times (H - T) = 0 \tag{19}$$

Since the vector $H - T$ can be expressed as the gradient of a scalar, i.e.

$$H = T - \nabla\Omega \tag{20}$$

where Ω is a magnetic scalar potential.
Also, since

$$\nabla \times E = -\frac{\partial B}{\partial t} \tag{21}$$

Then,

$$\nabla \times E = \nabla \times \left[\left(\frac{1}{\sigma} \right) \nabla \times T \right] \tag{22}$$

$$= -\frac{\partial B}{\partial t} = \mu_0 \mu_r \left(\frac{\partial}{\partial t} \right) (T - \nabla\Omega)$$

$$= -\mu_0 \mu_r \left(\frac{\partial T}{\partial t} \right) - \nabla\left(\frac{\partial \Omega}{\partial t} \right)$$

which finally reduces to the following two scalar equations[19, 20]:

$$\nabla^2 T - \mu\sigma \left(\frac{\partial T}{\partial t} \right) = -\mu\sigma\nabla\left(\frac{\partial \Omega}{\partial t} \right) \tag{23}$$

and

$$\nabla^2 \Omega = 0 \tag{24}$$

Due to the complex geometry, nonlinear property, and magnetic saturation effect, the design procedure and evaluation of accuracy of the proposed novel configuration became more complicated. It must be noted that for proper operation, the proposed configuration was expected to work under full saturation condition.

7.Simulation and magnetic optimization

To confirm the design procedure of the proposed LSRM and the precision of the analytical model, 2-D FE analysis is used. The inductances and flux linkages of the phase windings, normal forces, and propulsion developed by the proposed configuration are determined for various excitation currents and translator positions. It should be noted that FEA, in general, provides more accurate results than the magnetic analytical method with an equivalent circuit method because it considers a large number of flux paths as compared to the magnetic equivalent circuit method.

An accurate calculation of the magnetic field distribution is obtained using the Magnet CAD package (Infolytica Corporation Ltd). In order to obtain precise information about electromagnetic characteristics and magnetic behavior, such as inductance, propulsion force, and normal force for different positions, the proposed LSRM translator is shifted from an unaligned position, with respect to the stator, to an aligned position. This is done at different excitation currents and the normal force, inductance, and propulsion forces, corresponding to each translator position, are obtained.

- Magnetic optimization design methodology

An FEM analysis optimization routine for the optimum design of a proposed 6-10 LSRM for long stator applications has been set up, which includes two FE analyses procedure. The first one is an EM FE analysis for the translator and stator pole geometry to find the minimum force ripple at different aligned to unaligned positions. The second procedure involves EM FEA for the translator at a specified position to find the minimum translator weight and electromagnetic FEA. The design

optimization searches were implemented in a commercial Magnet CAD package (Infolytica Corporation Ltd., 2007).

The dimensional variables were: stator and translator tooth width and tooth height, which ranged between $h_{mt} = [22 - 27]$ mm, $h_{st} = [28 - 32]$ mm, $W_{mt} = [14 - 24]$mm, and $W_{st} = [W_{mt} \pm 0 - 2]$ mm, mover yoke thickness, and translator width. The rms current densities at low and high speeds were also set as variables. Airgap was fixed as 0.8 mm. The constraints were: maximum translator width

($\leq$ 80 mm) and maximum axial translator length ($\leq$ 500 mm). The objective was to maximize the average output force. The optimization was done for 6-10 LSRM.

Figure 4 shows the flux distributions inside the proposed 6-10 and conventional 6-4 LSRM for the fully aligned, half aligned, and unaligned positions with a phase current of 10A in one phase winding. It is observed that the leakage flux lines cross the stator slot air gap to the adjacent stator poles and complete their path through the stator back-irons.
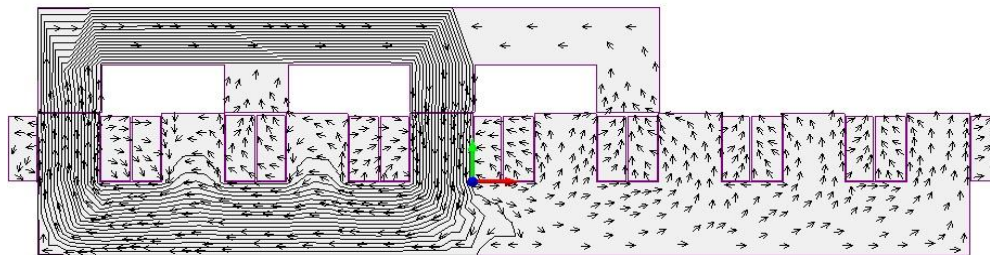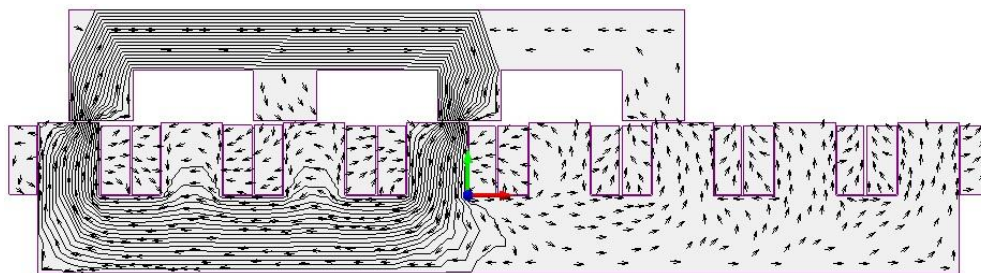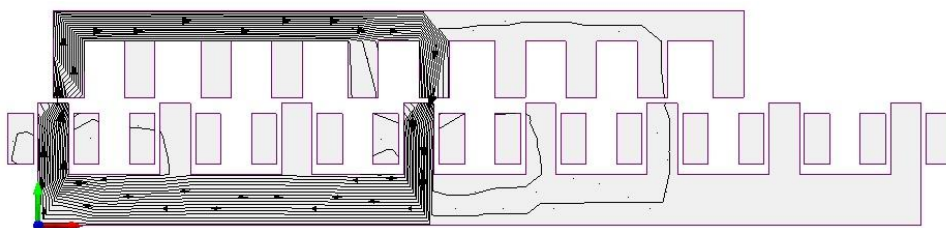

6-4 Configuration
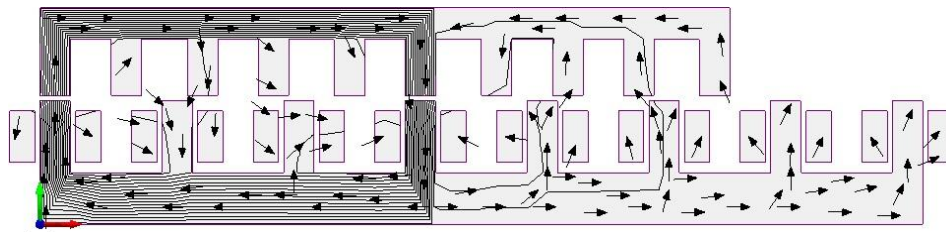
6-10 Configuration

(a) Fully aligned position

6-4 Configuration
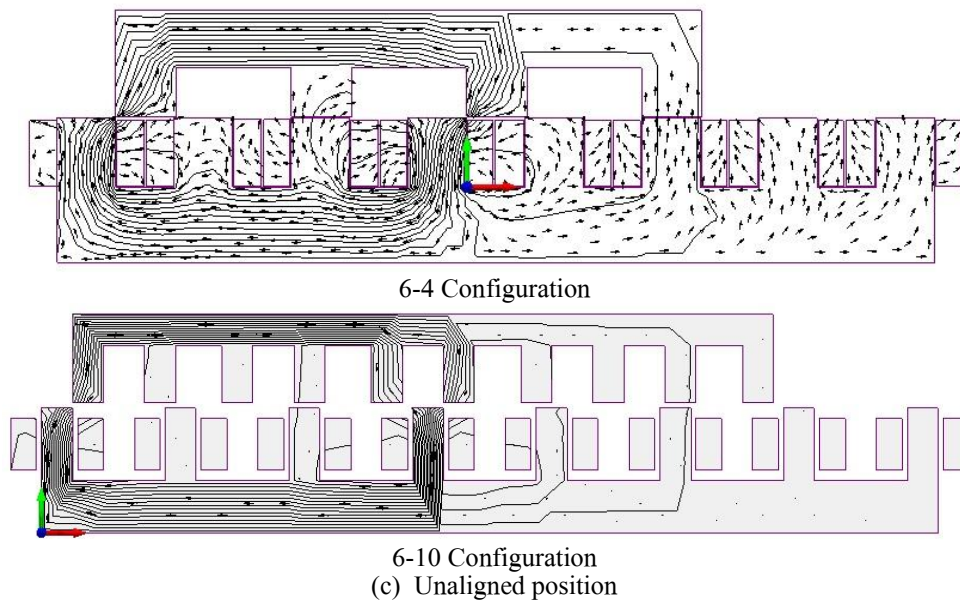
6-10 Configuration

(b) Half aligned position

6-4 Configuration

6-10 Configuration
(c) Unaligned position

Fig. 4. Flux distribution of the 3-Phase proposed 6-10 and conventional 6-4 LSRM at rated current, 10A for (a) fully aligned, (b) half aligned and (c) unaligned position

Figure 5 shows the inductance profile obtained from FEM and analytical results at 10 A phase current for various translator positions for both conventional 6-4 and proposed novel 6-10 LSRM configuration.

Figure 6 shows the flux linkage curve from analytical and FEM analysis with three different phase currents for various translator positions. A comparison of the FEA results and analytical analysis for flux linkage versus
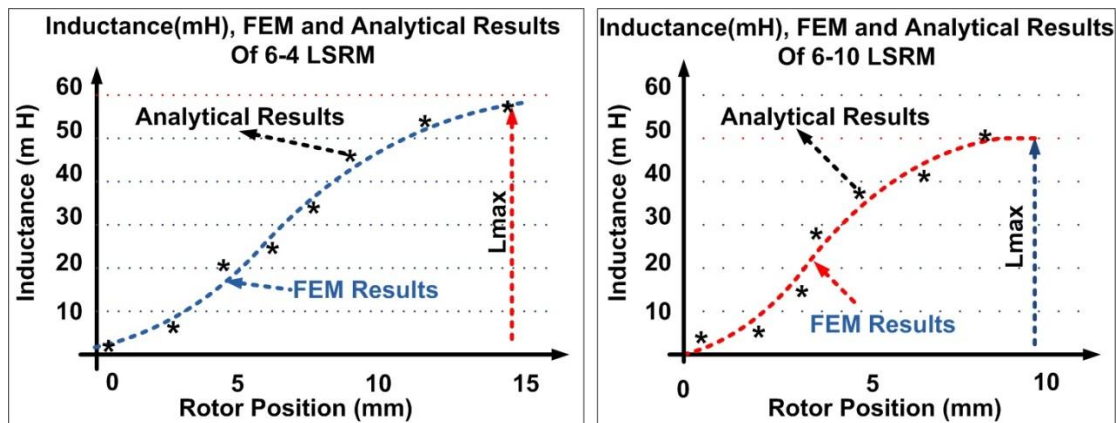

Fig. 5. Inductance curve for 6-4 and 6-10 LSRM configuration
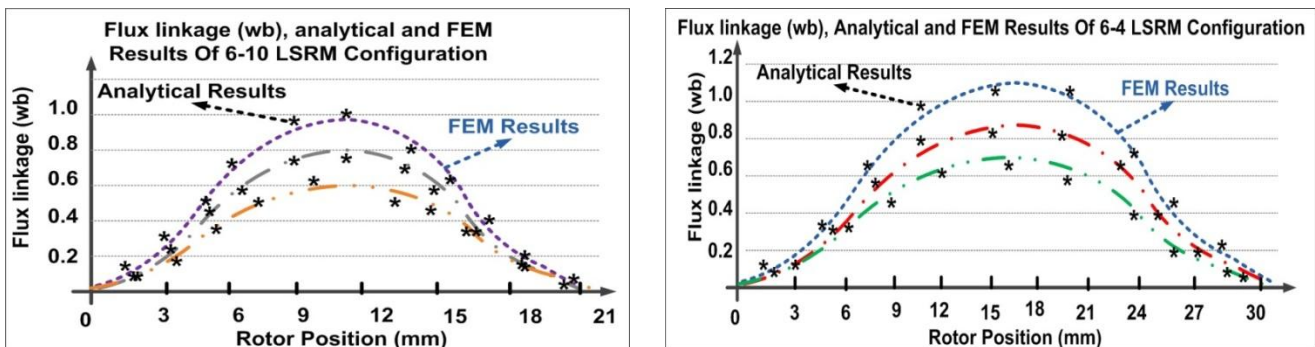FEA and Analytical simulation results of inductance at 10A, phase current

Fig. 6. FEM and Analytical Result of the flux linkage profile at several different phase currents with respect to various translator positions, 6-4 conventional and 6-10 proposed LSRM

current at various rotor positions in the 6-10 configuration LSRM is shown in Fig.7.

Figure 8 shows the propulsion force profile at different positions obtained from FEM analysis for both conventional 6-4 and the proposed 6-10 LSRM.

The obtained propulsion force profile from FEM analysis at different positions for the proposed 6-10 and conventional 6-4 LSRM are shown in Fig.8.

Figure 9 shows the obtained propulsion force profile from FEM analysis with three different phase currents for various translator positions for the proposed 6-10 LSRM.

Figures 10 and 11 show the output force for both 6-4 conventional and 6-10 proposed LSRM. It can be observed that the 6/10 proposed LSRM shows better output torque capabilities. From Table 6 it can be observed that the 6/10 proposed LSRM produces 28% – – 40% higher peak force. Also, from Table 7, it can be observed that the 6/10 proposed LSRM produces 35% – 47% higher average force.
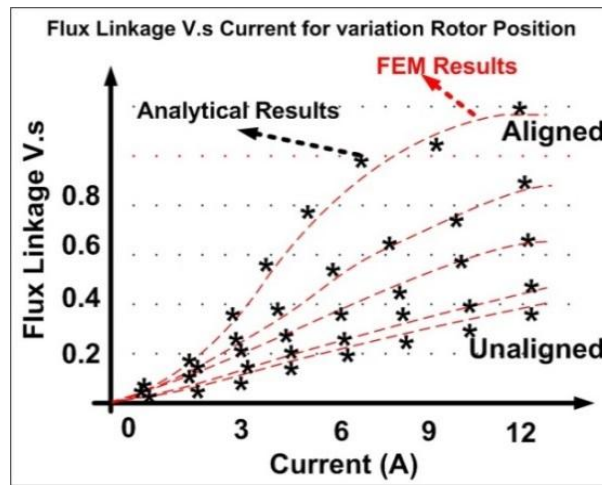

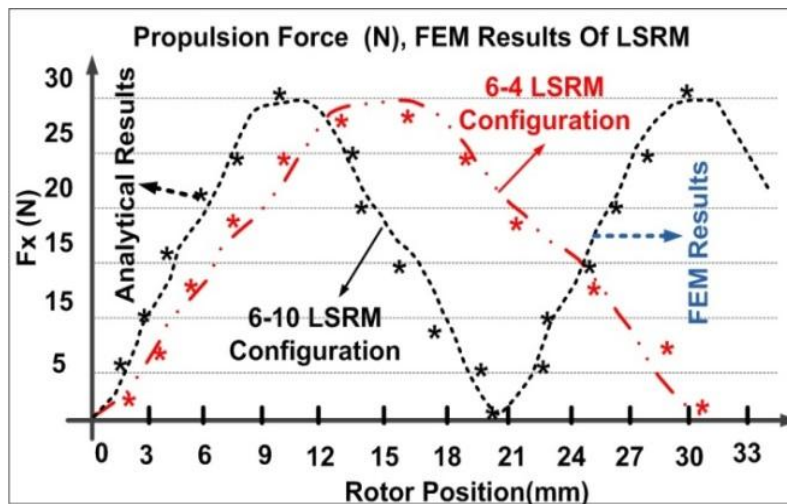**Fig.7.** Flux linkage V.s Current for variation rotor position for 6-10 configuration LSRM, FEM and Analytical results

Fig. 8. analytical and FEA simulation results of propulsion force at different position
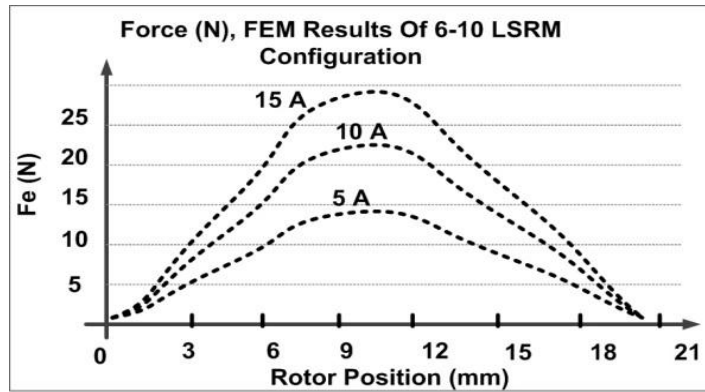
Fig. 9. FEA simulation results of propulsion force at different phase currents for 6-10 LSRM
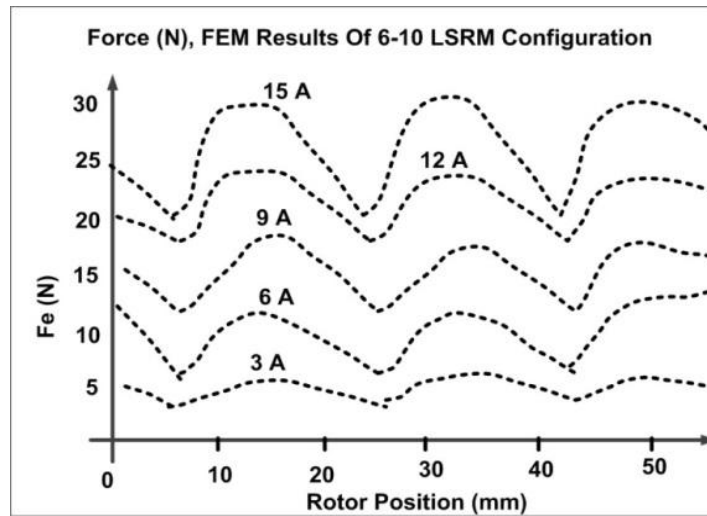

Fig. 10. FEA simulation results of propulsion force at different phase currents for 6-10 LSRM

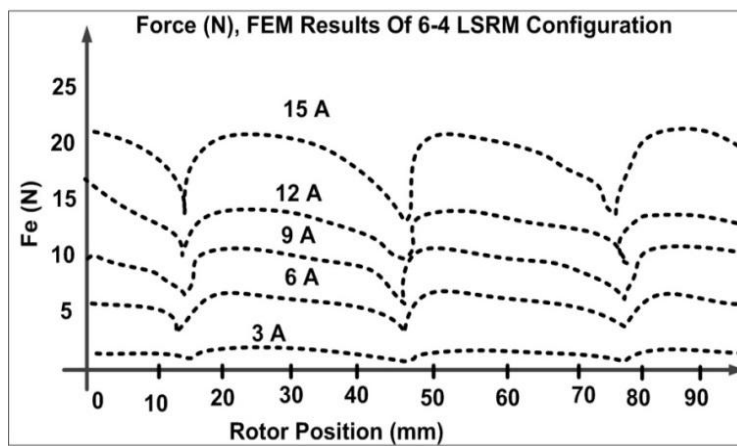**Fig. 11**. FEA simulation results of propulsion force at different phase currents for 6-4 LSRM

Table 6.Peak force comparison

Factor	Phase Current (A)	6-4 LSRM	6-10 LSRM	% Different
		PEAKE FORCE COMPARISON		
	3	2.5	3.2	28
	6	5.8	8.1	39
Peake Force	9	12.1	16.3	40
	12	13.8	20	39
	15	20	27	35

Table 7. Average force comparison

Factor	AVERAGE FORCE COMPARISON			
	Phase Current (A)	6-4 LSRM	6-10 LSRM	% Different
	3	2	2.7	35
	6	5.2	7.6	46
Average Force	9	11.6	15.8	36
	12	13.2	19.4	47
	15	19	26.4	38

Force ripple is defined from the instantaneous force F_i as the difference between the maximum and minimum forces, expressed as a percentage of the average force. This can be written as:

$$Force\ Ripple = \frac{Max(F_i) - Min(F_i)}{F_{ave}} \times 100\%$$

From Table 8, it can be observed that the 6/10 proposed LSRM produces -5.5% – 33.4% lower force ripple. Finally, Table 9 shows the comparison of geometric parameters.

8.Conclusion

This study deals with the designing and 2-D FE computations of the magnetic field distribution for a novel configuration linear switched reluctance (LSR) motor. Comparison of the calculated magnetic field and torque characteristics with their desired values illustrate the conformity of the design parameter's stage. It has been observed

through numerical analysis that the proposed configuration gives higher force and drastically reduced force ripple. From numerical analysis of the presented configuration, it has been observed that the proposed linear motor produces higher force per unit volume and similar force ripple when compared to a conventional 6-4 LSRM with almost identical number of stator tooth, number of phases, and constraints in volume.

References

[1] Krishnan K., Switched Reluctance Motor Drives, Modeling, Simulation, Analysis, Design, and Applications, CRC Press (2001).

[1] Baoming G., Almeida A. T., Ferreira F., Design of Transverse Flux Linear Switched Reluctance Motor, IEEE Transactions on Magnetics (2009) 45(1): 113–119.

[3] Ma C., Qu L., Multiobjective Optimization of Switched Reluctance

Table 8. Force ripple comparison

Factor	Force Ripple Comparison			
	Phase Current (A)	6-4 LSRM	6-10 LSRM	% Different
	3	25	18	28
	6	34	33	2.9
Force Ripple	9	18	19	-5.5
	12	13.6	10	26.4
	15	27	18	33.4

Table 9. Comparison of geometric parameters

Comparison of Geometric Parameters			
Parameters of Comparison	6-4 LSRM	6-10 LSRM	% Different
Cross sectional Area of Stator Tooth (mm^2)	1680	1200	28
Cross sectional Area of Rotor Tooth(mm^2)	1800	304	83
Cross sectional Area of Stator slot(mm^2)	1680	3300	96.4

Motors Based on Design of Experiments and Particle Swarm Optimization, IEEE Transactions on Energy Conversion, DOI: 10.1109/TEC.2015.2411677 (2015) (99):1-10.

[4] Jin Y. , Bilgin B., Emadi A., An Offline Torque Sharing Function for Torque Ripple Reduction in Switched Reluctance Motor Drives, IEEE Transactions on Energy Conversion (2015) 30(2): 726-735.

[5] Boldea I., Linear Electric Machines, Drives and MAGLEVs Handbook, CRC Press (2013).

[6] Amoros J. G., Andrada P., Sensitivity Analysis of Geometrical Parameters on a Double-Sided Linear Switched Reluctance Motor, IEEE Transactions on Industrial Electronics (2010) 57(1).

[7] Lim H. S., Krishnan R., Lobo N. S., Design and Control of a Linear Propulsion System for an Elevator Using Linear Switched Reluctance Motor Drives, IEEE Transactions on Industrial Electronics (2008)55(2): 534–542.

[8] Liu C.T., Su K.S., Chen J.W., Operational Stability Enhancement Analysis of a Transverse Flux Linear Switched-Reluctance Motor, in IEEE Transactions on Magnetics (2000) 36(5): 3699 – 3702.

[9] Yanni L., Aliprantis D.C., Optimum Stator Tooth Shapes for Torque Ripple Reduction in Switched Reluctance Motors, IEEE International Electric Machines & Drives Conference (IEMDC), DOI: 10.1109/IEMDC.2013.6556224 (2013) 1037 – 1044.

[10] Sheth N. K., Rajagopal K. R., Optimum Pole Arcs for a Switched Reluctance Motor for Higher Torque with Reduced Ripple, IEEE Transactions on Magnetics (2003) 39(5): 3214–3216.

[11] Lee J.W., Kim H.S., Kwon B., Kim B.T., New Rotor Shape Design for Minimum Torque Ripple of SRM Using FEM, IEEE Transactions Magnetics (2004) 40 (2): 754 - 757,.

[12] Mikail R., Husain I., Sozer Y., Islam M., Sebastian T.,Torque-Ripple Minimization of Switched Reluctance Machines Through Current Profiling, IEEE Transactions on Industry Applications (2013) 49 (3):1258 -1267.

[13] Husain I., Minimization of Torque Ripple in SRM Drive, IEEE Transactions on Industrial Electronics (2002) 49(1):28 -39.

[14] Lee D. H., Lee Z. G., Ahn J. W., A Simple Nonlinear Logical Torque Sharing Function for Low-Torque Ripple SR Drive, IEEE Transactions on Industrial Electronics (2009) 56(8): 3021 -3028.

[15] Kiwoo P., Liu X., Chen Z., A Non-Unity Torque Sharing Function for Torque Ripple Minimization of Switched Reluctance Generators, The European Conference on Power Electronics and Applications (2013) 1 -10.

[16] Choi Y.K, Koh C. S, Pole Shape Optimization of Switched Reluctance Motor for Reduction of Torque Ripple, 12th Biennial IEEE Conference on Electromagnetic Field Computation, DOI: 10.1109/CEFC-06.2006.1633125 (2006).

[17] Choi Y.K., Yoon H. S., Koh C. S., Pole-Shape Optimization of a Switched-Reluctance Motor for Torque Ripple Reduction, IEEE Transactions on Magnetics (2007) 43(4).

[18] Wang H., Lee D.H., Park T.H., Ahn J.W., Hybrid Stator-Pole Switched Reluctance Motor to Improve Radial Force for Bearing Less Application, Energy Convers Manage (2011)52:1371–6.

[19] Faghihi F., Heydari H., Reduction of Leakage Magnetic Field in Electromagnetic Systems Based on Active Shielding Concept Verified by Eigenvalue Analysis, Progress In Electromagnetics Research (2009) 96: 217-236.

[20] Rezaeealam J.B., Yamada S., Coupled Finite-Element/Boundary-Element Analysis Of A Reciprocating Self-Excited Induction Generator In A Harmonic Domain, IEEE Transactions On Magnetics (2005) 41(11).

[21] Tian J., Lv Z. Q., Shi X. W., Xu L., Wei F., An Efficient Approach for Multifrontal Algorithm to Solve Non-Positive-Definite Finite Element Equations In Electromagnetic Problems", Progress In Electromagnetics Research (2009) 95121-133.

[22] Norhisam M., Ridzuan S., Firdaus R. N., Aravind C. V., Wakiwaka H., Nirei M., Comparative Evaluation On Power-Speed Density Of Portable Permanent Magnet Generators For Agricultural Application, Progress In Electromagnetics Research (2012) 129:345-363.

[23] Jian L., Xu G., Gong Y., Song J., Liang J., Chang M., Electromagnetic Design And Analysis Of A Novel Magnetic-Gear-Integrated Wind Power Generator

Using Time-Stepping Finite Element Method, Progress In Electromagnetics Research(2011.)113:351-367.

[24] Mahmoudi A., Kahourzade S., Rahim N. A., Hew W. P., Ershad N. F., Slot-Less Torus Solid-Rotor-Ringed Line-Start Axial-Flux Permanent-Magnet Motor, Progress In Electromagnetics Research (2012) 131:331-355.

[25] Liang J., Jian L., Xu G., Shao Z., Analysis Of Electromagnetic Behavior in Switched Reluctance Motor for The Application Of Integrated Air Conditioner On-Board Charger System, Progress in Electromagnetics Research, (2012) 124:347-364.

[26] Dan-Cristian Popa, Vasile-Ioan Gliga, and Lorand Szabo, Theoretical and Experimental Study of a Modular Tubular Transverse Flux Reluc-Tance Machine, Progress in Electromagnetics Research (2013) 139:41-55.

[27] Cheshmehbeigi H. M., Afjei S. E., Nasiri B., Electromagnetic Design Based on Hybrid Analytical and 3-D Finite Element Method for Novel Two Layers Bldc Machine, Progress In Electromagnetics Research,DOI:10.2528/PIER12111301 (2013) 136: 141-155.

[28] Liu C., Chau K. T., Electromagnetic Design and Analysis of Double-Rotor Flux-Modulated Permanent-Magnet Machines, Progress in Electromagnetics Research (2012) 131:81-97.

[29] Li X., Chau K.T., Cheng M., Hua W., Comparison of Magnetic-Geared Permanent-Magnet Machines, Progress in Electromagnetics Research (2013) 133: 177-198.

[30] Jian L., Liang J., Shi Y., Xu G., A Novel Double-Winding Permanent Magnet Flux Modulated Machine for Stand-Alone Wind Power Generation, Progress In Electromagnetics Research (2013) 142: 275-289.

[31] Yan L., Zhang L., Wang T., Jiao Z., Chen C. Y., Chen I-M., Magnetic Field of Tubular Linear Machines with Dual Halbach Array, Progress in Electromagnetics Research (2013) 136: 283-299,.

[32] Kahourzade S., Gandomkar A., Mahmoudi A., Abd Rahim N., Hew W. P., Uddin M.N., Design Optimization and Analysis of AFPM Synchronous Machine in Corporating Density, Thermal analysis NDBACK-EMFTHD Progress in Electromagnetics Research (2013) 136: 327-367.

[33] Andreux R., Fontchastagner J., Takorabet N., Labbe N., Metral J.S., A General Approach for Brushed DC Machines Simulation Using a Dedicated Field/Circuit Coupled Method, Progress in Electromagnetics Research (2014) 145, 213-227.

[34] Musolino A., Rizzo R., Tripodi E., Tubular Linear Induction Machine as a Fast Actuator, Analysis and Design Criteria, Progress in Electromagnetics Research (2012) 132:603-619.

[35] Khalil A., Modeling and Analysis of Four Quadrant Sensorless Control of a Switched Reluctance Machine over the Entire Speed Range, Dissertation, University of Akron (2005).

[36] Rahman M., Chancharoensook P., Dynamic Modeling of a Four-Phase 8/6 Reluctance Motor Using Current and Torque Look-up Tables, IECON 02 (Industrial Electronics Society) 28th Annual Conference, IEEE 2002 .

[37] Ren Z., T-Ω Formulation for Eddy-Current Problems in Multiply Connected Regions, IEEE Transactions on Magnetics (2002) 38(2).

[38] Webb J. P., Singular Tetrahedral Finite Elements of High Order for Scalar Magnetic and Electric Field Problems, IEEE Transactions on Magnetics (2008) 44 (6).